

A NEW EVOLUTIONARY PATH TO TYPE IA SUPERNOVAE: HELIUM-RICH SUPER-SOFT X-RAY SOURCE CHANNEL

IZUMI HACHISU

Department of Earth Science and Astronomy, College of Arts and Sciences, University of Tokyo, Komaba,
 Meguro-ku, Tokyo 153-8902, Japan
 e-mail: hachisu@chianti.c.u-tokyo.ac.jp

MARIKO KATO

Department of Astronomy, Keio University, Hiyoshi, Kouhoku-ku, Yokohama 223-8521, Japan
 e-mail: mariko@educ.cc.keio.ac.jp

KEN'ICHI NOMOTO, AND HIDEYUKU UMEDA

Department of Astronomy, University of Tokyo, Bunkyo-ku, Tokyo 113-0033, Japan
 e-mail: nomoto@astron.s.u-tokyo.ac.jp, umeda@astron.s.u-tokyo.ac.jp
 Research Center for the Early Universe, University of Tokyo, Bunkyo-ku, Tokyo 113-0033, Japan

to be published in the Astrophysical Journal, 519, No.1

ABSTRACT

We have found a new evolutionary path to Type Ia supernovae (SNe Ia) which has been overlooked in previous work. In this scenario, a carbon-oxygen white dwarf (C+O WD) is originated, not from an asymptotic giant branch star with a C+O core, but from a red-giant star with a helium core of $\sim 0.8 - 2.0 M_{\odot}$. The helium star, which is formed after the first common envelope evolution, evolves to form a C+O WD of $\sim 0.8 - 1.1 M_{\odot}$ with transferring a part of the helium envelope onto the secondary main-sequence star. This new evolutionary path, together with the optically thick wind from mass-accreting white dwarf, provides a much wider channel to SNe Ia than previous scenarios. A part of the progenitor systems are identified as the luminous supersoft X-ray sources or the recurrent novae like U Sco, which are characterized by the accretion of helium-rich matter. The white dwarf accretes hydrogen-rich, helium-enhanced matter from a lobe-filling, slightly evolved companion at a critical rate and blows excess matter in the wind. The white dwarf grows in mass to the Chandrasekhar mass limit and explodes as an SN Ia. A theoretical estimate indicates that this channel contributes a considerable part of the inferred rate of SNe Ia in our Galaxy, i.e., the rate is about ten times larger than the previous theoretical estimates for white dwarfs with slightly evolved companions.

Subject headings: binaries: close — novae — stars: mass-loss — stars: supernovae — white dwarfs — X-rays: stars

1. INTRODUCTION

Type Ia supernovae (SNe Ia) have been widely believed to be a thermonuclear explosion of a mass-accreting white dwarf (WD) (e.g., Nomoto et al. 1997 for a recent review). However, the immediate progenitor binary systems have not been identified yet (Branch et al. 1995). There exist two models discussed frequently as progenitors of SNe Ia: 1) the Chandrasekhar (Ch) mass model, in which a mass-accreting carbon-oxygen (C+O) WD grows in mass up to the Ch mass and explodes as an SN Ia, and 2) the sub-Chandrasekhar (sub-Ch) mass model, in which an accreted layer of helium atop a C+O WD ignites off-center for a WD mass well below the Ch mass. The early time spectra of the majority of SNe Ia are in excellent agreement with the synthetic spectra of the Ch mass models, while the spectra of the sub-Ch mass models are too blue to be comparable with the observations (Höflich & Khokhlov 1996; Nugent et al. 1997).

For the evolution of accreting WDs toward the Ch mass, two scenarios have been proposed: 1) a double degenerate (DD) scenario, i.e., merging of double C+O WDs with a combined mass surpassing the Ch mass limit (Iben & Tutukov 1984; Webbink 1984), and 2) a single degenerate (SD) scenario, i.e., accretion of hydrogen-rich matter via mass transfer from a binary companion (e.g., Nomoto 1982a; Nomoto et al. 1994). The issue of DD vs. SD is

still debated (e.g., Branch et al. 1995), although theoretical modeling has indicated that the merging of WDs leads to the accretion-induced collapse rather than SN Ia explosion (Saio & Nomoto 1985, 1998; Segretain et al. 1997).

For the Ch/SD scenario, a new evolutionary model has been proposed by Hachisu, Kato, & Nomoto (1996; hereafter HKN96). HKN96 have shown that if the accretion rate exceeds a critical rate, the WD blows a strong wind and burns hydrogen steadily at this critical rate and expels excess matter in the wind. The WD increases its mass up to the Ch mass avoiding formation of a common envelope. Li & van den Heuvel (1997) have extended HKN96's model to a system consisting of a mass-accreting WD and a lobe-filling, more massive, main-sequence (MS) or sub-giant star (hereafter "WD+MS system"), identified with luminous supersoft X-ray sources, and found that such a system is one of the main progenitors of SNe Ia as well as a system consisting of a WD and a lobe-filling, less massive, red-giant (hereafter "WD+RG system") proposed by HKN96.

Recently, Yungelson & Livio (1998) have reanalyzed the models by HKN96 and Li & van den Heuvel based on their population synthesis code and concluded that both HKN96's WD+RG and Li & van den Heuvel's WD+MS systems can account for only (at most) 10% of the inferred rate of SNe Ia in our Galaxy. However, Yungelson & Livio (1998) overlooked important evolutionary processes

both in the WD+MS and WD+RG systems. In this paper, we first describe an important evolutionary process to form the WD+MS system, which has been overlooked in previous works (e.g., Di Stefano & Rappaport 1994; Yungelson et al. 1996; Yungelson & Livio 1998). Another evolutionary process leading to the WD+RG system is discussed elsewhere (Hachisu, Kato, & Nomoto 1999, hereafter HKN99). In §2, we describe the new evolutionary process to form the WD+MS system. Including this new evolutionary path, we will show that the secondary (slightly evolved MS star) becomes a helium-rich star like in U Sco (e.g., Williams et al. 1981), which is transferring helium-rich matter onto the primary (WD). We have reanalyzed such a helium-rich matter accretion onto the WD based on the optically thick wind theory developed by Kato & Hachisu (1994). If the secondary MS star has a mass of $\sim 2 - 3.5M_\odot$, a WD with an initial mass of $0.8 - 1.1M_\odot$ grows in mass to the Ch mass and explodes as an SN Ia. We describe the evolution of such a WD+MS system in §3. The new parameter region thus obtained is much wider than that by Li & van den Heuvel (1997) and Yungelson & Livio (1998). Discussions follow in §4, in which we have estimated the realization frequency of our WD+MS systems that accounts for about a third of the inferred rate of SNe Ia in our Galaxy.

2. FORMATION OF A NAKED HELIUM CORE AND ITS EVOLUTION TOWARD C+O WHITE DWARF

In this section, we describe the evolutionary path to form the WD+MS system where the secondary (MS star) has a helium-rich envelope. This important evolutionary path shown in Figure 1 has been overlooked in previous work. Yungelson & Livio (1998) applied their population synthesis code to the WD+MS systems and found that the realization frequency of the WD+MS systems is at most one tenth of the inferred rate of SNe Ia in our Galaxy. In their population synthesis code, they consider only initial systems consisting of a more massive AGB star with a C+O core and a less massive main-sequence star. This system undergoes a common envelope evolution and finally yields a binary system of a mass-accreting C+O WD and a lobe-filling MS or sub-giant star. Their code does not include another important evolutionary path, in which a more massive component fills up its inner critical Roche lobe when it develops a *helium core* of $\sim 0.8 - 2.0M_\odot$ in its *red-giant phase*.

2.1. Common Envelope Evolution at Red-Giant Phase with a Helium Core

This evolutionary path from *stage A* to *F* in Figure 1 has been first introduced by Hachisu & Kato (1999) to explain the helium-rich companion of the recurrent nova U Sco. We consider, for example, a close binary at a separation a with the primary of mass $M_{1,i} = 7M_\odot$ and the secondary of $M_{2,i} = 2M_\odot$ (*stage A*). When the primary has evolved to a red-giant of the radius R_1 forming a helium core of mass $M_{1,\text{He}}$ (*stage B*), it fills up its inner critical Roche lobe, i.e., $R_1 = R_1^*$. Here, R_1^* is the effective radius of the inner critical Roche lobe of the primary, which is approximated by Eggleton's (1983) formula,

$$\frac{R_1^*}{a} = f(q) \equiv \frac{0.49q^{2/3}}{0.6q^{2/3} + \ln(1 + q^{1/3})}, \quad (1)$$

for the mass ratio $q = M_1/M_2$. The long dashed line in Figure 2 shows the primary radius R_1 against the helium core mass $M_{1,\text{He}}$ (Bressan et al. 1993). The radius of the primary increases with the helium core mass from $M_{1,\text{He}} \sim 0.2M_\odot$ to $\sim 1.4M_\odot$ until helium burning ignites at the center of the helium star. If the primary fills its inner critical Roche lobe at a certain $M_{1,\text{He}}$, i.e., $R_1(M_{1,\text{He}}) = R_1^*$, the separation of the binary, a , is given by

$$a = \frac{R_1(M_{1,\text{He}})}{f(q)}. \quad (2)$$

Using this relation, we can plot the initial separation a_i against $M_{1,\text{He}}$ as shown by the thick solid line in Figure 2.

Then the mass transfer begins. This mass transfer is dynamically unstable because the primary red-giant star has a convective envelope. The binary undergoes common envelope (CE) evolution (*stage C*), which yields a much more compact close binary consisting of a naked helium star of $M_{1,\text{He}}$ and a main-sequence star of $M_2 = 2M_\odot$ (*stage D*). Figure 2 shows the separation $a_{f,\text{CE}}$ and the inner critical Roche lobe radius of the secondary $R_{2,f,\text{CE}}^*$ after the common envelope evolution. Here, we assume the relation

$$\frac{a_{f,\text{CE}}}{a_i} \sim \alpha_{\text{CE}} \cdot \left(\frac{M_{1,\text{He}}}{M_{1,i}} \right) \cdot \left(\frac{M_2}{M_{1,i} - M_{1,\text{He}}} \right), \quad (3)$$

with the efficiency $\alpha_{\text{CE}} = 1.0$ for the common envelope evolution (e.g., Iben & Tutukov 1984; Iben & Livio 1993; Yungelson & Livio 1998).

After the common envelope evolution, the radii of the inner critical Roche lobes of the primary and the secondary become $R_1^* \sim 0.36a_{f,\text{CE}}$ and $R_2^* \sim 0.4a_{f,\text{CE}}$, respectively. Since the secondary radius (shown by the dashed line in Figure 2 for the $2M_\odot$ ZAMS) should be smaller than its inner critical Roche lobe, i.e., $R_2 < R_{2,f,\text{CE}}^*$, the initial separation a_i should exceed $\sim 80 R_\odot$ as shown in Figure 2. The upper bound of the initial separation is obtained from the maximum radius of the $7M_\odot$ star which has formed a helium core, i.e., $a_i \approx 2R_{1,\text{max}} \lesssim 2 \times 300 R_\odot$. Thus, the allowable range of the initial separations for our model is $80 R_\odot \lesssim a_i \lesssim 600 R_\odot$, so that $R_1^* \sim 1.4 - 18 R_\odot$ and $R_2^* \sim 1.6 - 20 R_\odot$ for the case of Figure 2.

2.2. Transfer of Helium Envelope to the Secondary

After the hydrogen-rich envelope is stripped away and hydrogen shell burning vanishes, the naked helium core contracts to ignite central helium burning and becomes a helium main sequence star of mass $M_{1,\text{He}}$ (*stage D*). For $M_{1,\text{He}} \lesssim 2M_\odot$, its C+O core mass is less than $1.07M_\odot$ which is the lower mass limit to the non-degenerate carbon ignition (e.g., Umeda et al. 1999; Nomoto & Hashimoto 1988 for a review). Then the helium star forms a degenerate C+O core, whose mass $M_{\text{C+O}}$ grows by helium shell burning. When $M_{\text{C+O}}$ becomes $0.9 - 1.0M_\odot$ and the core becomes strongly degenerate, its helium envelope expands to $R_1 \sim 1.4 - 18 R_\odot$ (e.g., Paczynski 1971a; Nomoto 1982b) to fill its inner critical Roche lobe again (*stage E*). Helium is transferred to the secondary stably on an *evolutionary time scale* of $\tau_{\text{EV}} \sim 10^5$ yr because the mass

ratio is smaller than 0.79 ($q = M_1/M_2 < 0.79$). The resultant mass transfer (MT) rate is $\dot{M}_1 \sim 10^{-5} M_\odot \text{ yr}^{-1}$, which is too low to form a common envelope (e.g., Neo et al. 1977; Kippenhahn & Meyer-Hofmeister 1977). After the helium envelope is lost, the primary becomes a C+O WD of $M_{\text{WD}} \sim 0.9 - 1.1 M_\odot$ (*stage F*). In Figure 3, $M_{1,f,\text{MT}} = M_{\text{WD}}$ is plotted as a function of $M_{1,\text{He}}$. Here, we assume the relation of (in solar mass units of M_\odot)

$$M_{\text{WD}} = \begin{cases} 0.2(M_{1,\text{He}} - 0.85) + 0.85, & \text{for } 0.85 < M_{1,\text{He}} \lesssim 2, \\ M_{1,\text{He}}, & \text{for } 0.46 \lesssim M_{1,\text{He}} \leq 0.85, \end{cases} \quad (4)$$

for the final degenerate C+O WD mass vs. the initial helium star mass relation (reduced from the evolutionary paths by Paczynski 1971a and Nomoto 1982b). Helium stars with $M_{\text{He}} \leq 0.85 M_\odot$ do not expand to $\sim 2 - 10 R_\odot$, thus burning most of helium to C+O without transferring helium to the secondary. For $M_{1,\text{He}} \gtrsim 2.0 M_\odot$, the C+O core has a mass larger than $1.07 M_\odot$ before becoming degenerate, thus igniting carbon to form an O+Ne+Mg core (e.g., Nomoto 1984), thus we do not include their mass range. For $M_{1,\text{He}} \lesssim 0.46 M_\odot$, helium is not ignited to form a C+O core.

The secondary increases its mass M_2 by receiving almost pure helium matter of $\Delta M_{\text{He}} \sim 0.1 - 0.6 M_\odot$, which is a function of $M_{1,\text{He}}$ as plotted in Figure 3. Then a helium-enriched envelope is formed as illustrated in Figure 1 (*stage F*). After the helium mass transfer (MT), the separation increases by 10%–40%, i.e., $a_{f,\text{MT}} \sim (1.1 - 1.4)a_{f,\text{CE}} \sim (4 - 70) R_\odot$. Here, we assume the conservation of the total mass and angular momentum during the helium mass transfer, which leads to the relation of

$$\frac{a_{f,\text{MT}}}{a_{f,\text{CE}}} = \left(\frac{M_{1,\text{He}}}{M_{1,\text{He}} - \Delta M_{\text{He}}} \right)^2 \left(\frac{M_{2,i}}{M_{2,i} + \Delta M_{\text{He}}} \right)^2, \quad (5)$$

and we use this to obtain $a_{f,\text{MT}}$ and then the orbital period $P_0 \equiv P_{f,\text{MT}}$ in Figure 3.

Since the secondary receives $\sim 0.1 - 0.6 M_\odot$ helium, its hydrogen content in the envelope decreases to $X \sim 0.6$ if helium is completely mixed into the central part of the star. However, the envelope of the mass-receiving star is not convective but radiative so that the helium content may be higher in the outer part of the star.

2.3. Helium-Enriched Main-Sequence Companion

We have examined total $5 \times 5 = 25$ cases, $M_{1,i} = 4, 5, 6, 7, 9 M_\odot$ and $M_{2,i} = 1.0, 1.5, 2.0, 2.5, 3.0 M_\odot$, and have found the possible progenitors to be in the range of $M_{1,\text{C+O WD}} \sim 0.8 - 1.1 M_\odot$ and $M_{2,\text{MS}} \sim 1.7 - 3.5 M_\odot$ with the separation of $a_{f,\text{MT}} \sim 4 - 80 R_\odot$. In these cases, the secondary forms a helium-enriched envelope for the primary mass of $M_{1,\text{WD}} \sim 0.9 - 1.1 M_\odot$ (but not for $M_{1,\text{WD}} \sim 0.8 - 0.85 M_\odot$). We assume, in this paper, that the average mass fractions of hydrogen and helium in the envelope are $X = 0.50$ and $Y = 0.48$ respectively. (assuming the solar abundance of heavy elements $Z = 0.02$). For the $9 M_\odot + 2.5 M_\odot$ case, much more helium is transferred, while much less helium is transferred for the $6 M_\odot + 2 M_\odot$ case (see Table 1).

3. GROWTH OF C+O WHITE DWARFS

Starting from a close binary of $M_{\text{WD},0} \equiv M_{1,\text{C+O WD}} \sim 0.8 - 1.1 M_\odot$ and $M_{\text{MS},0} \equiv M_{2,\text{MS}} \sim 1.7 - 3.5 M_\odot$ with the separation of $a_0 \equiv a_{f,\text{MT}} \sim 4 - 80 R_\odot$, we have followed a growth of the WD component to examine whether the WD reaches $1.38 M_\odot$ and explodes as an SN Ia (from *stage F* to *J* in Fig. 4).

The initial secondary now has a helium-rich envelope (*stage F*). It evolves to expand and fills its inner critical Roche lobe near the end of main-sequence (MS) phase. Then, it starts mass transfer (*stage G*). This is a *case A* mass transfer after Kippenhahn & Weigert (1967, also Paczynski 1971b) or a *cataclysmic-like mass transfer* after Iben & Tutukov (1984). Since the donor is more massive than the accretor (WD component), the separation decreases and the inner critical Roche lobe decreases even to scrape the envelope mass off the donor star. Thus, the mass transfer proceeds on a *thermal time scale* rather than an evolutionary time scale (*stage H*). The transferred matter is helium-rich as observed in the recurrent nova U Sco.

3.1. Optically Thick Winds from Mass-Accreting White Dwarfs

Hachisu, Kato, & Nomoto (1996, HKN96) have shown that optically thick winds blow from the white dwarf when the mass accretion rate exceeds a critical value (*stage H*). In the present case, the accreted matter to form the white dwarf envelope is helium-rich, which is different from the solar abundance in HKN96. Assuming $X = 0.50$, $Y = 0.48$, and $Z = 0.02$, we have calculated the envelope models of accreting white dwarfs for various accretion rates and white dwarf masses, i.e., $M_{\text{WD}} = 0.6, 0.7, 0.8, 0.9, 1.0, 1.1, 1.2, 1.3, 1.35$, and $1.377 M_\odot$. Optically thick winds occur for all these ten cases of M_{WD} as shown for five cases of $M_{\text{WD}} = 0.8, 1.0, 1.2, 1.3$, and $1.377 M_\odot$ in Figures 5 and 6. Our numerical methods have been described in Kato & Hachisu (1994). The envelope solution is uniquely determined if the envelope mass M_{env} is given, where M_{env} is the mass above the base of the hydrogen-burning shell. Therefore, the wind mass loss rate \dot{M}_{wind} and the nuclear burning rate \dot{M}_{nuc} are obtained as a function of the envelope mass M_{env} , i.e., $\dot{M}_{\text{wind}}(M_{\text{env}})$ and $\dot{M}_{\text{nuc}}(M_{\text{env}})$ as shown in Figure 5.

The envelope mass of the white dwarf is determined by

$$\dot{M}_{\text{env}} = \dot{M}_2 - (\dot{M}_{\text{wind}} + \dot{M}_{\text{nuc}}). \quad (6)$$

If the mass transfer rate does not change much in a thermal time scale of the WD envelope, the steady-state $\dot{M}_{\text{env}} = 0$, i.e.,

$$\dot{M}_2 = \dot{M}_{\text{wind}} + \dot{M}_{\text{nuc}}, \quad (7)$$

is a good approximation. In such a steady-state approximation, the ordinates in Figures 5 and 6, $\dot{M}_{\text{wind}} + \dot{M}_{\text{nuc}}$, are regarded as the mass transfer rate from the secondary \dot{M}_2 . Thus, the envelope solution is determined from the relation in Figure 5 for the given mass transfer rate \dot{M}_2 . The photospheric radius, temperature, and velocity are also obtained from the relations in Figure 6.

Optically thick winds blow when the mass transfer rate exceeds the critical rate, which corresponds to the break of each solid line in Figure 5. There exists only a static (no

wind) envelope solution for the mass transfer rate below this break. Its critical accretion rate is approximated as

$$\dot{M}_{\text{cr}} = 1.2 \times 10^{-6} \left(\frac{M_{\text{WD}}}{M_{\odot}} - 0.40 \right) M_{\odot} \text{ yr}^{-1}, \quad (8)$$

for $X = 0.50$, $Y = 0.48$ and $Z = 0.02$. If the mass accretion rate exceeds the critical rate, i.e., $\dot{M}_2 > \dot{M}_{\text{cr}}$, the strong wind blows from the white dwarf. The white dwarf accretes helium almost at the critical rate, i.e., $\dot{M}_{\text{nuc}} \approx \dot{M}_{\text{cr}}$, and expels the excess matter in the wind at a rate of $\dot{M}_{\text{wind}} \approx \dot{M}_2 - \dot{M}_{\text{cr}}$. Here, we assume that the white dwarf accretes helium-rich matter from the equator via the accretion disk and blows winds to the pole or off the equator.

3.2. Efficiency of Mass-Accretion in Hydrogen Shell Burning

Steady hydrogen shell burning converts hydrogen into helium atop the C+O core, which can be regarded as a helium matter accretion onto the C+O WD. To estimate whether or not the white dwarf mass grows to $1.38M_{\odot}$, we must calculate the mass accumulation efficiency, that is, the ratio between the mass accumulated in the WD after H/He-burning and the mass transferred from the companion. We denote the efficiency by η_{H} and η_{He} for hydrogen shell-burning and helium shell-burning, respectively. As shown in the previous subsection, the excess matter is blown in the wind when the mass transfer rate exceeds the critical rate, which leads to $\eta_{\text{H}} = (\dot{M}_2 - \dot{M}_{\text{wind}})/\dot{M}_2 < 1$, for the wind phase.

During the evolution of mass-accreting white dwarfs, the accretion rate becomes lower than \dot{M}_{cr} in some cases. Then the wind stops (*stage I* in Fig. 4). Hydrogen steadily burns for $\dot{M}_2 > \dot{M}_{\text{st}} \approx 0.5\dot{M}_{\text{cr}}$. Then, we have $\eta_{\text{H}} = 1$. For $\dot{M}_2 < \dot{M}_{\text{st}}$, hydrogen shell-burning becomes unstable to trigger weak shell flashes. Once a weak hydrogen shell flash occurs, a part of the envelope mass of the white dwarf may be lost from the system (e.g., Kovetz & Prialnik 1994). In the present study, no mass loss is assumed during the weak hydrogen shell flashes until the mass transfer rate becomes lower than $\dot{M}_{\text{low}} = 1 \times 10^{-7} M_{\odot} \text{ yr}^{-1}$, i.e., $\eta_{\text{H}} = 1$ for $\dot{M}_{\text{low}} \lesssim \dot{M}_2 < \dot{M}_{\text{st}}$. When the mass transfer rate becomes lower than \dot{M}_{low} , however, no mass accumulation is expected from such relatively strong hydrogen shell-flashes (e.g., Kovetz & Prialnik 1994), i.e., $\eta_{\text{H}} = 0$ for $\dot{M}_2 \lesssim \dot{M}_{\text{low}}$. Therefore, we stop calculating the binary evolution either when the primary reaches $1.38M_{\odot}$ (*stage J* in Fig. 4), i.e., $M_{1,\text{WD}} = 1.38M_{\odot}$ or the mass transfer rate becomes lower than \dot{M}_{low} .

To summarize, we have used the following simplified relation

$$\eta_{\text{H}} = \begin{cases} (\dot{M}_2 - \dot{M}_{\text{wind}})/\dot{M}_2 < 1, & (\dot{M}_{\text{cr}} < \dot{M}_2 < 1 \times 10^{-4} M_{\odot} \text{ yr}^{-1}) \\ 1, & (\dot{M}_{\text{low}} \leq \dot{M}_2 \leq \dot{M}_{\text{cr}}) \\ 0, & (\dot{M}_2 \leq \dot{M}_{\text{low}}) \end{cases} \quad (9)$$

for the mass accumulation efficiency of hydrogen shell burning.

3.3. Efficiency of Mass-Accretion in Helium Shell Burning

For $\dot{M}_2 \geq \dot{M}_{\text{cr}}$, steady hydrogen burning is equivalent to the helium accretion at the critical rate of \dot{M}_{cr} given by equation (8). In this case, weak helium shell flashes are triggered (e.g., Kato et al. 1989) and almost all processed matter is accumulated on the C+O WD. Recently, Kato & Hachisu (1999) have recalculated the helium wind model after the helium shell flashes and estimated the mass accumulation efficiency with the updated OPAL opacity (Iglesias & Rogers 1996). Here, we adopt their new results in a simple analytic form, i.e.,

$$\eta_{\text{He}} = \begin{cases} 1, & (-5.9 \leq \log \dot{M}_{\text{He}} \lesssim -5) \\ -0.175(\log \dot{M}_{\text{He}} + 5.35)^2 + 1.05, & (-7.8 < \log \dot{M} < -5.9) \end{cases} \quad (10)$$

where the helium mass accretion rate, \dot{M}_{He} , is in units of $M_{\odot} \text{ yr}^{-1}$. We use this formula for various white dwarf masses and accretion rates, although their results are given only for the $1.3M_{\odot}$ white dwarf (Kato & Hachisu 1999).

The wind velocity in helium shell flashes reaches as high as $\sim 1000 \text{ km s}^{-1}$ (Kato & Hachisu 1999), which is much faster than the orbital velocities of our WD+MS binary systems $a\Omega_{\text{orb}} \sim 300 \text{ km s}^{-1}$. It should be noted that either a Roche lobe overflow or a common envelope does not play a role as a mass ejection mechanism because the envelope matter goes away quickly from the system without interacting with the orbital motion (see Kato & Hachisu 1999 for more details).

3.4. Mass Transfer Rate of the Secondary

We have followed binary evolutions from the initial state of $(M_{\text{WD},0}, M_{\text{MS},0}, a_0)$ or $(M_{\text{WD},0}, M_{\text{MS},0}, P_0)$, where P_0 is the initial orbital period. Here, the subscript naught (0) denotes *stage F* in Figure 4, that is, before the mass transfer from the secondary starts. The radius and luminosity of slightly evolved main-sequence stars are calculated from the analytic form given by Tout et al. (1997). The mass transfer proceeds on a thermal time scale for the mass ratio of $M_2/M_1 > 0.79$. We approximate the mass transfer rate as

$$\dot{M}_2 = \frac{M_2}{\tau_{\text{KH}}} \cdot \max \left(\frac{\zeta_{\text{RL}} - \zeta_{\text{MS}}}{\zeta_{\text{MS}}}, 0 \right), \quad (11)$$

where τ_{KH} is the Kelvin-Helmholtz timescale (e.g., Paczynski 1971b), and $\zeta_{\text{RL}} = d \log R^*/d \log M$ and $\zeta_{\text{MS}} = d \log R_{\text{MS}}/d \log M$ are the mass-radius exponents of the inner critical Roche lobe and the main sequence component, respectively (e.g., Hjellming & Webbink 1987). The effective radius of the inner critical Roche lobe, R^* , is calculated from equation (1).

3.5. Late Binary Evolution toward SN Ia

The separation is determined by

$$\frac{\dot{a}}{a} = \frac{\dot{M}_1 + \dot{M}_2}{M_1 + M_2} - 2 \frac{\dot{M}_1}{M_1} - 2 \frac{\dot{M}_2}{M_2} + 2 \frac{j}{J}. \quad (12)$$

We estimate the total mass and angular momentum losses by the winds as

$$\dot{M} \equiv \dot{M}_1 + \dot{M}_2 = \dot{M}_{\text{wind}}, \quad (13)$$

and

$$\frac{\dot{J}}{J} = \ell \cdot \frac{(M_1 + M_2)^2}{M_1 M_2} \frac{\dot{M}}{M}, \quad (14)$$

where ℓ is a numeric factor expressing the specific angular momentum of the wind, i.e.,

$$\frac{\dot{J}}{M} = \ell \cdot a^2 \Omega_{\text{orb}}. \quad (15)$$

For the very fast winds such as $v_{\text{wind}} \gtrsim 2a\Omega_{\text{orb}}$, the wind has, on average, the same specific angular momentum as that of the WD component, i.e.,

$$\ell = \left(\frac{M_2}{M_1 + M_2} \right)^2, \quad (16)$$

because the wind is too fast to interact with the orbital motion (see also HKN99). In equations (12)–(15), we must take into account the sign of the mass loss rates, i.e., $\dot{M} = \dot{M}_{\text{wind}} \leq 0$, $\dot{M}_2 \leq 0$, $\dot{J} \leq 0$, and so on.

Figure 7 shows an example of such close binary evolutions which lead to the SN Ia explosion. Here, we start the calculation when the secondary fills its inner critical Roche lobe. The initial parameters are $M_{\text{WD},0} = 1.0M_{\odot}$, $M_{\text{MS},0} = 2.0M_{\odot}$, and $a_0 = 9.6R_{\odot}$ ($P_0 = 2.0$ d). The mass transfer begins at a rate as high as $\dot{M}_2 = 2.2 \times 10^{-6}M_{\odot} \text{ yr}^{-1}$. The WD burns hydrogen to form a helium layer at the critical rate of $\dot{M}_{\text{cr}} = 0.7 \times 10^{-6}M_{\odot} \text{ yr}^{-1}$ and the wind mass loss rate is $\dot{M}_{\text{wind}} = 1.5 \times 10^{-6}M_{\odot} \text{ yr}^{-1}$. Thus a large part of the transferred matter is blown off in the wind.

Since the mass ratio M_2/M_1 decreases, the mass transfer rate determined by equation(11) gradually decreases below \dot{M}_{cr} . The wind stops at $t = 1.9 \times 10^5$ yr. The mass transfer rate becomes lower than $\dot{M}_{\text{st}} \sim 5 \times 10^{-7}M_{\odot} \text{ yr}^{-1}$ (for $M_{\text{WD}} = 1.2M_{\odot}$) at $t = 3.8 \times 10^5$ yr and very weak shell flashes may occur. The WD mass gradually grows to reach $1.38M_{\odot}$ at $t = 6.7 \times 10^5$ yr. At this time, the mass transfer rate is still as high as $\dot{M}_2 = 3.6 \times 10^{-7}M_{\odot} \text{ yr}^{-1}$, because the mass ratio M_2/M_1 is still larger than 0.79, implying thermally unstable mass transfer.

This WD+MS system may not be observed in X-rays during the strong wind phase due to the self-absorption of X-rays. However, it is certainly identified as a luminous supersoft X-ray source from $t = 1.9 \times 10^5$ yr to 3.8×10^5 yr, because it is in a steady hydrogen shell burning phase without a strong wind. Just before the explosion, it may be observed as a recurrent nova like U Sco, which indicates a helium-rich accretion in quiescence (Hanes 1985).

3.6. Outcome of Late Binary Evolution

Thus we have obtained the final outcome of close binary evolutions for various sets of $(M_{\text{WD},0}, M_{\text{MS},0}, a_0)$ or $(M_{\text{WD},0}, M_{\text{MS},0}, P_0)$. Figure 8 depicts the final outcomes in the $M_{\text{MS},0} - \log P_0$ plane for $M_{\text{WD},0} = 1.1M_{\odot}$. Final outcome is either

- 1) forming a common envelope (denoted by \times) because the mass transfer rate at the beginning is large enough to form a common envelope, i.e., $R_{1,\text{ph}} > a \sim 10R_{\odot}$ for $\dot{M}_2 \gtrsim 1 \times 10^{-4}M_{\odot} \text{ yr}^{-1}$ as seen in Figure 6,

- 2) triggering an SN Ia explosion (denoted by \oplus , \bigcirc , or \odot) when $M_{1,\text{WD}} = 1.38M_{\odot}$, or
- 3) triggering repeated nova cycles (denoted by Δ), i.e., $\dot{M}_2 < \dot{M}_{\text{low}}$ when $M_{1,\text{WD}} < 1.38M_{\odot}$.

Among the SN Ia cases, the wind status at the explosion depends on \dot{M}_2 as follows.

- 2a) wind continues at the SN Ia explosion for $\dot{M}_{\text{cr}} < \dot{M}_2 \lesssim 1 \times 10^{-4}M_{\odot} \text{ yr}^{-1}$ (denoted by \oplus).
- 2b) wind stops before the SN Ia explosion but the mass transfer rate is still high enough to keep steady hydrogen shell burning for $\dot{M}_{\text{st}} < \dot{M}_2 < \dot{M}_{\text{cr}}$ (\bigcirc).
- 2c) wind stops before the SN Ia explosion and the mass transfer rate decreases to between $\dot{M}_{\text{low}} < \dot{M}_2 < \dot{M}_{\text{st}}$ at the SN Ia explosion (\odot).

The region producing an SN Ia is bounded by $M_{\text{MS},0} = 1.8 - 3.2M_{\odot}$ and $P_0 = 0.5 - 5$ d as shown by the solid line.

- i) The left bound is determined by $R_{2,f,\text{CE}}^* = R_2(\text{ZAMS})$ in Figure 2, where $R_2(\text{ZAMS})$ is the minimum radius of the secondary at the zero age main-sequence (ZAMS).
- ii) The right bound corresponds to the maximum radius at the end of main sequence, after which central hydrogen burning vanishes and the star shrinks.
- iii) The lower bound is determined by the decrease in the mass transfer rate mainly because the secondary mass decreases to reach the mass ratio M_2/M_1 below unity, i.e., $\dot{M}_2 < \dot{M}_{\text{low}}$.
- iv) The upper bound is limited by the formation of a common envelope. When the mass transfer rate is as high as a few times $10^{-5}M_{\odot} \text{ yr}^{-1}$ or more, the photosphere of the white dwarf envelope reaches the secondary and then swallows it, i.e., $R_{1,\text{ph}} \gtrsim a$ (see Fig. 6). It may be regarded as the formation of a common envelope. The binary will undergo a common envelope evolution and will not become an SN Ia.

The final outcome of the evolutions is also plotted in Figures 9–11 for other initial white dwarf masses of $M_{\text{WD},0} = 1.0M_{\odot}$, $0.9M_{\odot}$, and $0.8M_{\odot}$, respectively. Figure 12 shows the regions that lead to an SN Ia for all the white dwarf masses of $M_{\text{WD},0} = 0.75, 0.8, 0.9$, and $1.1M_{\odot}$ (thin solid lines) together with $M_{\text{WD},0} = 1.0M_{\odot}$ (thick solid line). The region for $M_{\text{WD},0} = 0.7M_{\odot}$ vanishes. The shrinking of the upper bound for smaller $M_{\text{WD},0}$ is due to larger initial mass ratio of $M_{\text{MS},0}/M_{\text{WD},0}$, which enhances the mass transfer rate at the beginning of mass transfer (*stage G*), thus resulting in the formation of a common envelope. The shrinking of the lower bound can be understood as follows: The white dwarf with smaller $M_{\text{WD},0}$ needs to accrete more mass from the slightly evolved main-sequence companion. Thus the companion's mass near the *stage I* or *J* (just before SN Ia explosion) is smaller after a considerable part of the hydrogen-rich envelope is transferred to supply hydrogen-rich matter to the white dwarf. The

thermal time scale of the companion is longer for smaller masses, thereby decreasing the mass transfer rate down to the nova region.

4. DISCUSSIONS

We have estimated the rate of SNe Ia originating from our WD+MS systems in our Galaxy by using equation (1) of Iben & Tutukov (1984), i.e.,

$$\nu = 0.2 \cdot \Delta q \cdot \int_{M_A}^{M_B} \frac{dM}{M^{2.5}} \cdot \Delta \log A \quad \text{yr}^{-1}, \quad (17)$$

where Δq and $\Delta \log A$ denote the appropriate ranges of the initial mass ratio and the initial separation, respectively, and M_A and M_B are the lower and the upper limits of the primary mass that leads to SN Ia explosions, respectively. For the WD+MS progenitors, we assume that $a_i \lesssim 1500 R_\odot$ in order to obtain a relatively compact condition of $a_{f,CE}$ after the common envelope evolution.

If the $\sim 1M_\odot$ C+O WD is a descendant from an AGB star, its zero-age main sequence mass is $\sim 7M_\odot$ (see, e.g., eq.(11) of Yungelson et al. 1995) and the binary separation is larger than $a_i \sim 1300 R_\odot$ (e.g., Iben & Tutukov 1984). Its separation shrinks to $a_{f,CE} \sim 60 R_\odot$ after the common envelope evolution for the case of $\alpha_{CE} = 1$ and $\sim 2M_\odot$ secondary. Then the orbital period becomes $P_0 \sim 30$ d, which is too long to become an SN Ia (e.g., Li & van den Heuvel 1997; see also Fig. 9). Therefore, the WD+MS systems descending from an AGB star may be rare as pointed out by Yungelson & Livio (1998) and may not be a main channel to SNe Ia.

To obtain the realization frequency of our WD+MS system descending from a red-giant with a helium core, we have followed total ~ 500 evolutions with the different initial set of $(M_{1,i}, M_{2,i}, a_i)$ and estimated the appropriate range for the initial separation of $\Delta \log A = \log a_{i,\max} - \log a_{i,\min}$ for total $5 \times 5 = 25$ cases of $(M_{1,i}, M_{2,i})$, each for the primary mass of $M_{1,0} = 4, 5, 6, 7$, and $9M_\odot$ and the secondary mass of $M_{2,0} = 1, 1.5, 2, 2.5$, and $3M_\odot$ (see Table 1). In Table 1, we omit the case of $M_{1,0} = 4M_\odot$ because it never leads to SN Ia explosions. We find that SN Ia explosions occur for the ranges of $M_{1,i} = 5.5 - 8.5M_\odot$, $M_{2,i} = 1.8 - 3.4M_\odot$, and $\Delta \log A = 0.5$. We thus obtain the realization frequency of SNe Ia from the WD+MS systems as $\nu_{MS} = 0.0010 \text{ yr}^{-1}$ for $\alpha_{CE} = 1$, by substituting $\Delta q = 3.4/5.5 - 1.8/8.5 = 0.41$, $M_A = 5.5M_\odot$, $M_B = 8.5M_\odot$, and $\Delta \log A = 0.5$ into equation (17). For comparison, we have obtained a realization frequency of SNe Ia for $\alpha_{CE} = 0.3$. It is still as high as $\nu_{MS} \sim 0.0007 \text{ yr}^{-1}$, which is about one fourth of the inferred rate. Our new rate of $\nu_{MS} = 0.0010 \text{ yr}^{-1}$ is about a third of the inferred rate of SNe Ia in our Galaxy and much higher than $\nu_{MS} = 0.0002 \text{ yr}^{-1}$ (as an upper limit) obtained by Yungelson & Livio (1998). The reason of their low frequency is probably due to the absence of the path through the pri-

mary's helium star phase in their scenarios. However, it should be noted here that Yungelson & Livio (1998) have also obtained a realization frequency of $\nu_{MS} \sim 0.001 \text{ yr}^{-1}$ under the assumption of no restrictions in their binary evolutions, the conditions of which are unlikely.

A part of our WD+MS systems are identified as the luminous supersoft X-ray sources (SSSs) (van den Heuvel et al. 1992). SSSs are characterized by a luminosity of $\sim 10^{38} \text{ erg s}^{-1}$ and a temperature of $T \sim 4 \times 10^5 \text{ K}$ ($kT \sim 35 \text{ eV}$), which have been established as a new class of X-ray sources through ROSAT observations (e.g., Kahabka & van den Heuvel 1997 for a recent review). A population synthesis for SSSs has first been done by Rappaport, Di Stefano, & Smith (1994), followed by a more complete population synthesis (Yungelson et al. 1996). These calculations predict the total number of the Galactic SSSs of ~ 1000 and led to the conclusion that the SSS birth rate is roughly consistent with the observation (e.g., Kahabka & van den Heuvel 1997 for a review). Our SN Ia progenitors should be observed as an SSS during the steady hydrogen shell burning phase without winds, which is about a few times 10^5 yr as shown in Figure 7. Then the number of SSSs from our scenario is roughly estimated to be at least about $\sim 3 \times 10^5 \text{ yr} \times \nu_{MS} \approx 300$, which should be added to 1000 by Yungelson et al. (1996). The total number is still consistent with observations.

Our WD+MS progenitor model predicts helium-enriched matter accretion onto a WD. Strong He II $\lambda\lambda 4686$ lines are prominent in the luminous supersoft X-ray sources (e.g., Kahabka & van den Heuvel 1997 for a recent review) as well as in the recurrent novae like U Sco (Hanes 1985; Johnston & Kulkarni 1992) and V394 CrA (Sekiguchi et al. 1989). Thus the weakness of the hydrogen emission lines relative to the He II and CNO lines is very consistent with the requirement that the accreted matter and hence the envelope of the secondary have a hydrogen-poor (helium-rich) composition.

For SNe Ia, several attempts have been made to detect signature of circumstellar matter. There has been no radio detections so far. Radio observations of SN 1986G have provided the most stringent upper limit to the circumstellar density as $\dot{M}/v_{10} = 1 \times 10^{-7} M_\odot \text{ yr}^{-1}$ (Eck et al. 1995), where v_{10} means $v_{10} = v/10 \text{ km s}^{-1}$. This is still 10 – 100 times higher than the density predicted for the white dwarf winds, because the WD wind velocity is as fast as $\sim 1000 \text{ km s}^{-1}$. Further attempts to detect high velocity hydrogen signature are encouraged.

We thank the anonymous referee for helpful comments to improve the manuscript. This research has been supported in part by the Grant-in-Aid for Scientific Research (05242102, 06233101, 08640321, 09640325) and COE Research (07CE2002) of the Japanese Ministry of Education, Science, Culture, and Sports.

REFERENCES

- Branch, D., Livio, M., Yungelson, L.R., Boffi, F.R., & Baron, E. 1995, PASP, 107, 717
- Bressan, A., Fagotto, F., Bertelli, G., & Chiosi, C. 1993, A&AS, 100, 647
- Di Stefano, R., & Rappaport, S. 1994, ApJ, 437, 733
- Eck, C.R., Cowan, J.J., Roberts, D.A., Boffi, F.R., & Branch, D. 1995, ApJ, 451, L53
- Eggleton, P. P. 1983, ApJ, 268, 368
- Hachisu, I., & Kato, M. 1999, ApJ, submitted (U Sco)
- Hachisu, I., Kato, M., & Nomoto, K. 1996, ApJ, 470, L97 (HKN96)
- Hachisu, I., Kato, M., & Nomoto, K. 1999, ApJ, submitted (HKN99)

- Hanes, D. A. 1985, MNRAS, 213, 443
Hjellming, M. S., & Webbink, R. F. 1987, ApJ, 318, 794
Höfllich, P., & Khokhlov, A. 1996, ApJ, 457, 500
Iben, I. Jr., & Livio, M. 1993, PASP, 105, 1373
Iben, I. Jr., & Tutukov, A. V. 1984, ApJS, 54, 335
Iglesias, C. A., & Rogers, F. 1996, ApJ, 464, 943
Johnston, H. M., & Kulkarni, S. R. 1992, ApJ, 396, 267
Kahabka, P., & van den Heuvel, E. P. J. 1997, ARA&A, 35, 69
Kato, M., Hachisu, I., 1994, ApJ, 437, 802
Kato, M., & Hachisu, I., 1999, ApJ, 513, in press (astro-ph/9901080)
Kato, M., Saio, H., & Hachisu, I. 1989, ApJ, 340, 509
Kippenhahn, R., & Meyer-Hofmeister, E. 1977, A&A, 54, 539
Kippenhahn, R., & Weigert, A. 1967, Z. Ap., 65, 251
Kovetz, A., & Prialnik, D. 1994, ApJ, 424, 319
Li, X.-D., & van den Heuvel, E. P. J. 1997, A&A, 322, L9
Neo, S., Miyaji, S., Nomoto, K., & Sugimoto, D. 1977, PASJ, 29, 249
Nomoto, K. 1982a, ApJ, 253, 798
Nomoto, K. 1982b, in Supernovae: A Survey of Current Research, ed. M. Rees & R. J. Stoneham (Dordrecht: Reidel), 205
Nomoto, K. 1984, ApJ, 277, 791
Nomoto, K., & Hashimoto, M. 1988, Phys. Rep., 163, 13
Nomoto, K., Iwamoto, K., & Kishimoto, N. 1997, Science, 276, 1378
Nomoto, K., Yamaoka, H., Shigeyama, T., Kumagai, S., & Tsujimoto, T. 1994, in Supernovae (Les Houches, Session LIV), ed. S. Bludman et al. (Amsterdam: Elsevier Sci. Publ.), 199
Nugent, P., Baron, E., Branch, D., Fisher, A., & Hauschildt, P. H. 1997, ApJ, 485, 812
Paczynski, B. 1971a, Acta Astronomica, 21, 1
Paczynski, B. 1971b, ARA&A, 9, 183
Rappaport, S., Di Stefano, R., & Smith, J. D. 1994, ApJ, 426, 692
Saio, H., & Nomoto, K. 1985, A&A, 150, L21
Saio, H., & Nomoto, K. 1998, ApJ, 500, 388
Sekiguchi, K., Catchpole, R. M., Fairall, A. P., Feast, M. W., Kilkenny, D., Laney, C. D., Lloyd Evans, T., Marang, F., & Parker, Q. A. 1989, MNRAS, 236, 611
Segretain, L., Chabrier, G., & Mochkovitch, R. 1997, ApJ, 481, 355
Tout, C. A., Aarseth, S. J., Pols, O. R., & Eggleton, P. P. 1997, MNRAS, 291, 732
Umeda, H., Nomoto, K., Yamaoka, H., & Wanajo, S. 1999, ApJ, 513, in press (astro-ph/9806336)
van den Heuvel, E. P. J., Bhattacharya, D., Nomoto, K., & Rappaport, S. 1992, A&A, 262, 97
Webbink, R. F. 1984, ApJ, 277, 355
Williams, R. E., Sparks, W. M., Gallagher, J. S., Ney, E. P., Starrfield, S. G., & Truran, J. W. 1981, ApJ, 251, 221
Yungelson, L., & Livio, M. 1998, ApJ, 497, 168
Yungelson, L., Livio, M., Truran, J. W., Tutukov, A., & Fedorova, A. 1996, ApJ, 466, 890
Yungelson, L., Livio, M., Tutukov, A., & Kenyon, S. 1995, ApJ, 447, 656

TABLE 1
INITIAL SEPARATIONS THAT LEAD TO TYPE IA SUPERNOVA EXPLOSIONS ($X = 0.50$ AND $Z = 0.02$).

	$5M_{\odot}$		$6M_{\odot}$		$7M_{\odot}$		$9M_{\odot}$	
	$\alpha_{CE} = 1$	0.3	$\alpha_{CE} = 1$	0.3	$\alpha_{CE} = 1$	0.3	$\alpha_{CE} = 1$	0.3
ΔM_{He}^a	—	—	0.0,0.0	0.0,0.2	0.1,0.2	0.37,0.37	0.5,0.6	0.6,0.6
$1.0M_{\odot}$	—	—	—	—	—	—	—	—
$1.5M_{\odot}$	—	—	—	—	—	—	—	—
$2.0M_{\odot}$	—	—	1.9,2.4 ^b	2.4,2.6	1.8,2.3	2.3,2.8	—	—
$2.5M_{\odot}$	—	—	1.8,2.4	2.3,2.7	1.8,2.3	2.4,2.8	1.8,2.3	2.4,2.5
$3.0M_{\odot}$	—	2.3,2.5	2.1,2.4	2.4,2.7	2.0,2.3	—	—	—

^ahelium mass transferred to the secondary in solar mass units, (minimum, maximum)

^binitial separation of $\log(a_i/R_{\odot})$, (minimum, maximum)

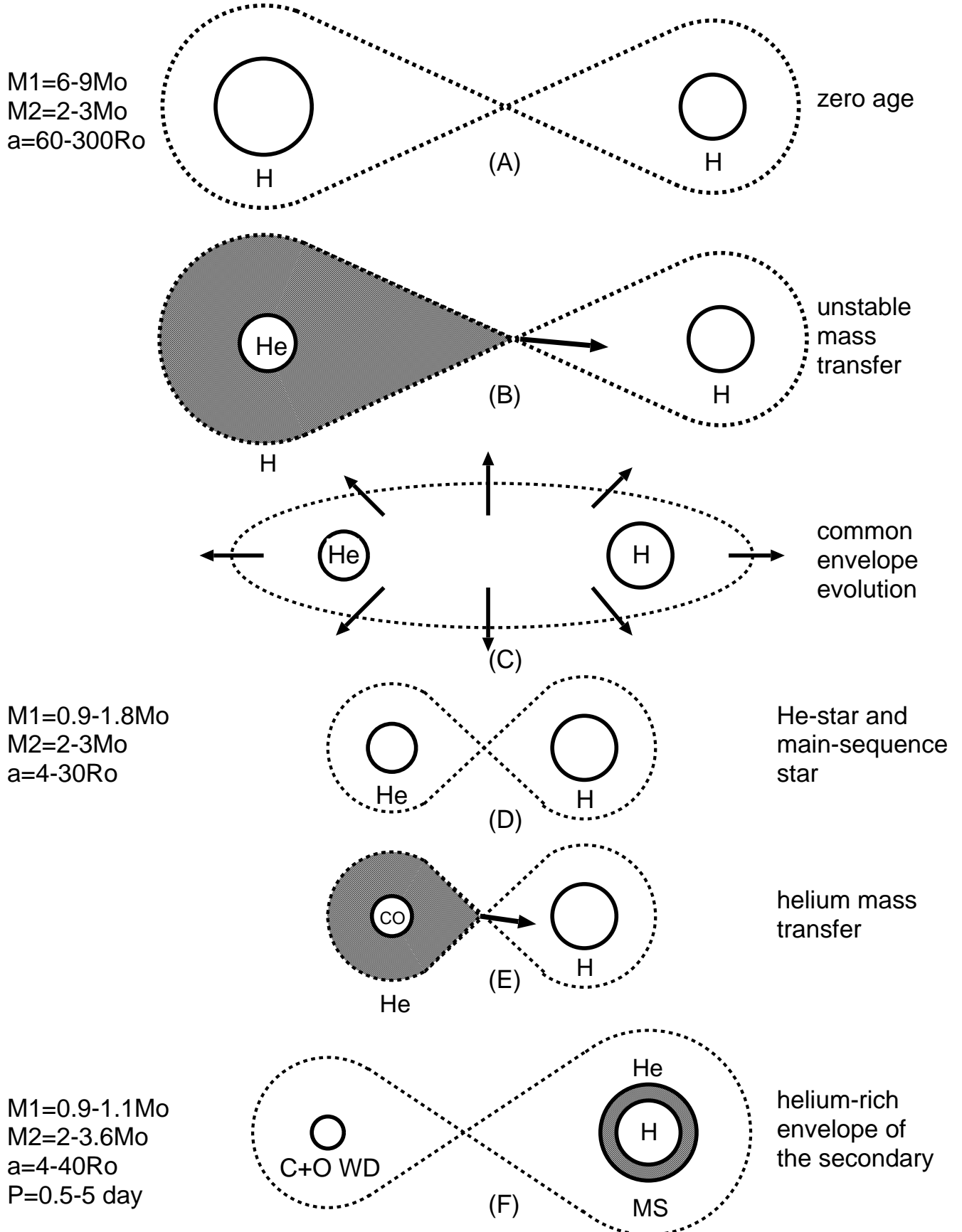


FIG. 1.— Early evolutionary path through the common envelope evolution to the helium matter transfer.

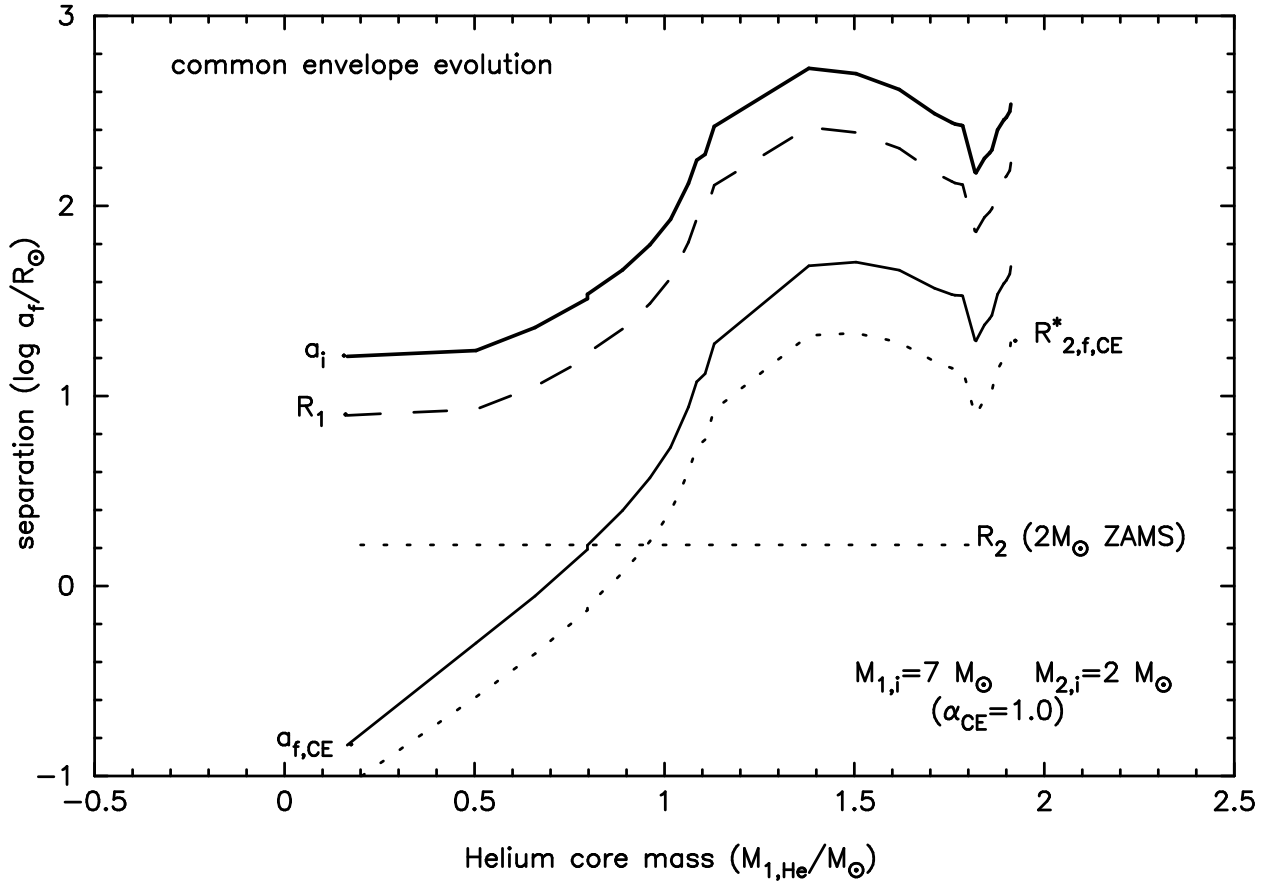


FIG. 2.— Long dashed line shows the radius of the primary R_1 against its helium core mass $M_{1,\text{He}}$. The radius increases with the helium core mass but it begins to decrease after helium is ignited at the center of the helium core when $M_{1,\text{He}} \sim 1.4M_{\odot}$. If the lobe-filling condition is satisfied, we obtain the separation a_i from equation (2). The thick and thin solid lines show the separations a_i (at stage B in Fig. 1) and $a_{f,\text{CE}}$ (at stage D) before and after the common envelope evolution, respectively, for the $7M_{\odot} + 2M_{\odot}$ pair. The separation shrinks by about a factor of ten after the common envelope evolution. Dotted horizontal line indicates the radius of $2M_{\odot}$ star at the zero age main-sequence (ZAMS). The helium core mass can grow in mass for the larger separation a_i , i.e., for the larger Roche lobe $R_{1,i}^*$.

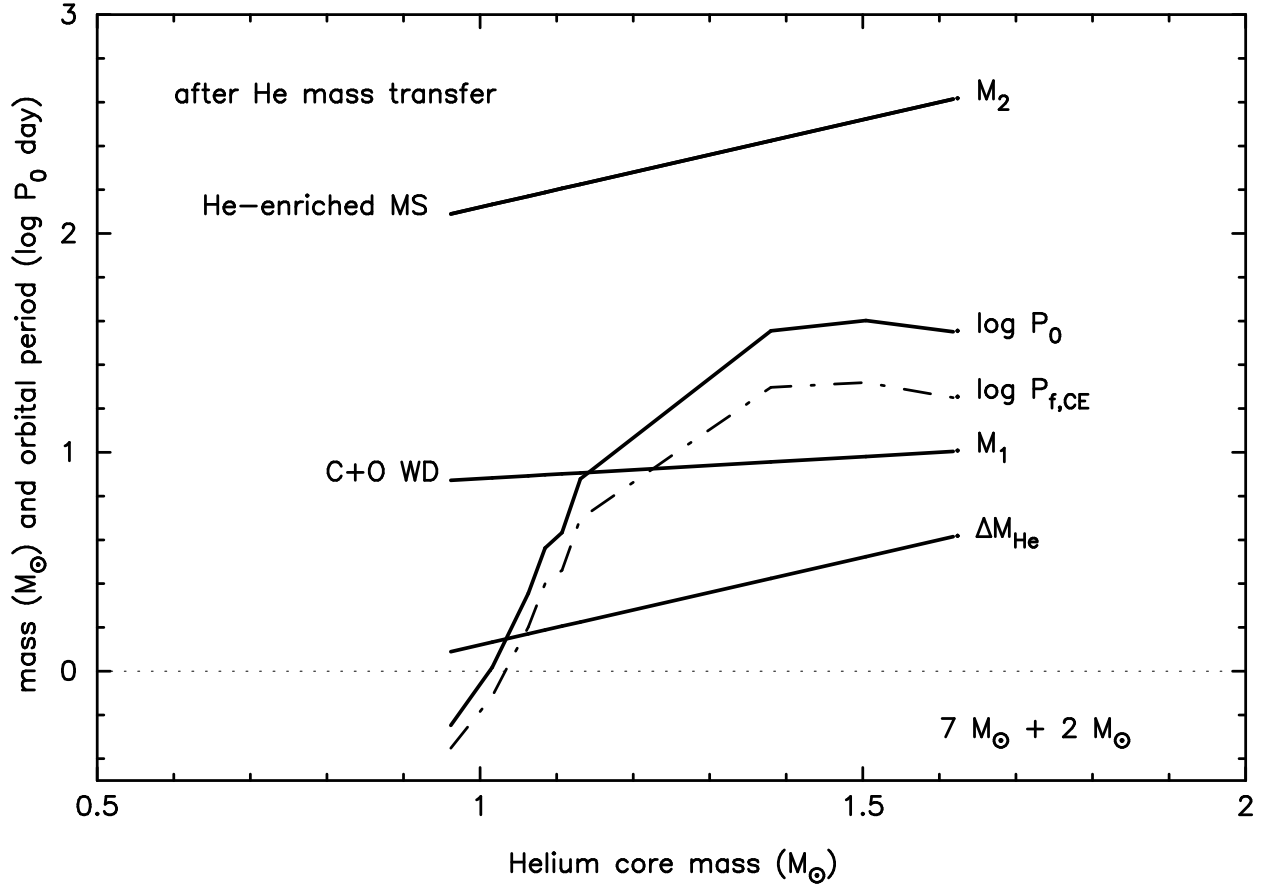


FIG. 3.— Thick solid lines show the mass of the primary (C+O WD) M_1 , the mass of the secondary (helium-enriched MS) M_2 , the mass transferred to the secondary ΔM_{He} , and the orbital period $\log P_0$ after the helium mass transfer (*stage F*) against the helium core mass at the beginning of helium mass transfer (*stage E*). The Dash-dotted line indicates the orbital period at the beginning of helium mass transfer (*stage E*). The separation increases and the orbital period also increases after the helium mass transfer.

$M_1 = 0.9 - 1.1 M_\odot$
 $M_2 = 2 - 3.6 M_\odot$
 $a = 4 - 40 R_\odot$
 $P = 0.5 - 5 \text{ day}$

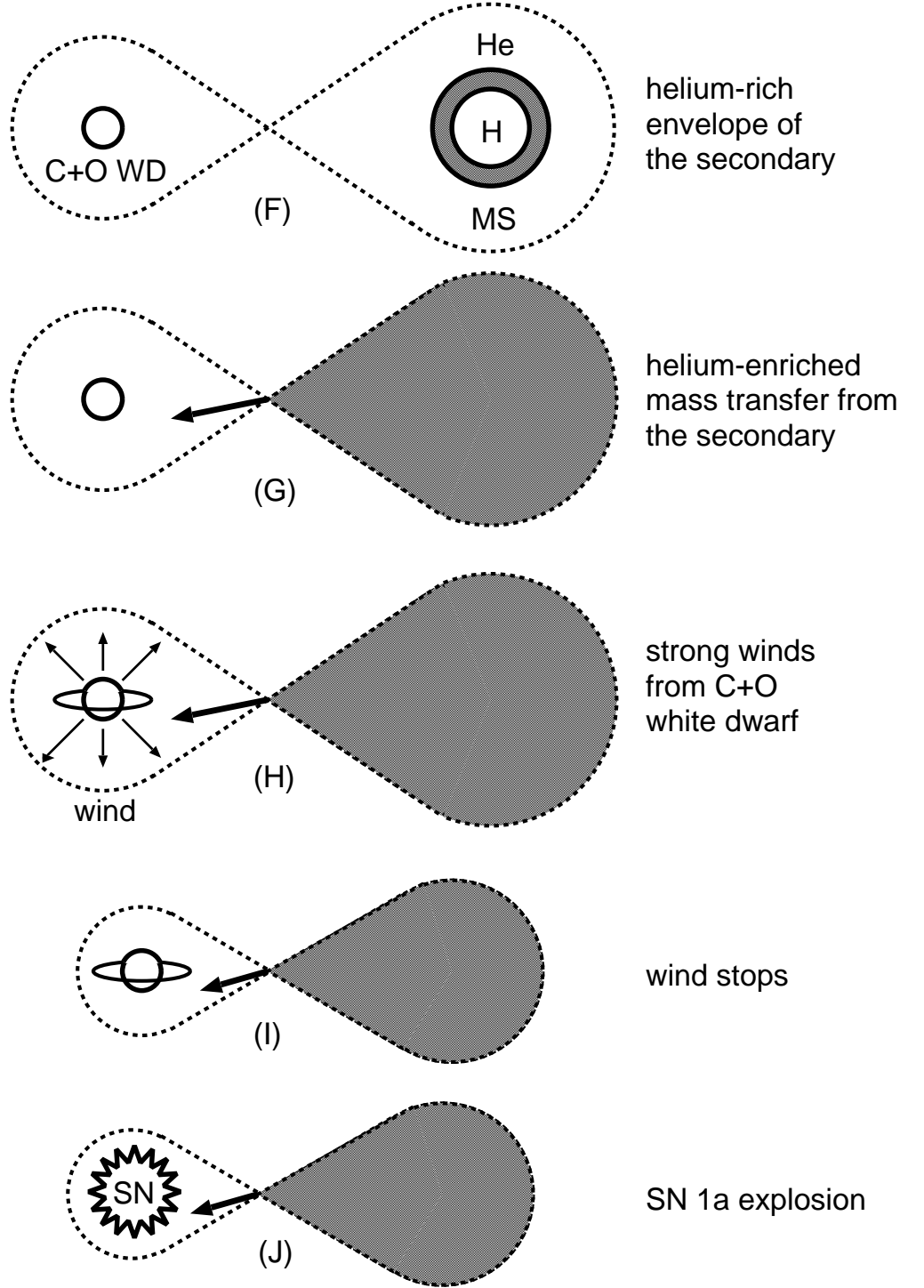


FIG. 4.— Late evolutionary path to an SN Ia explosion in our wind model.

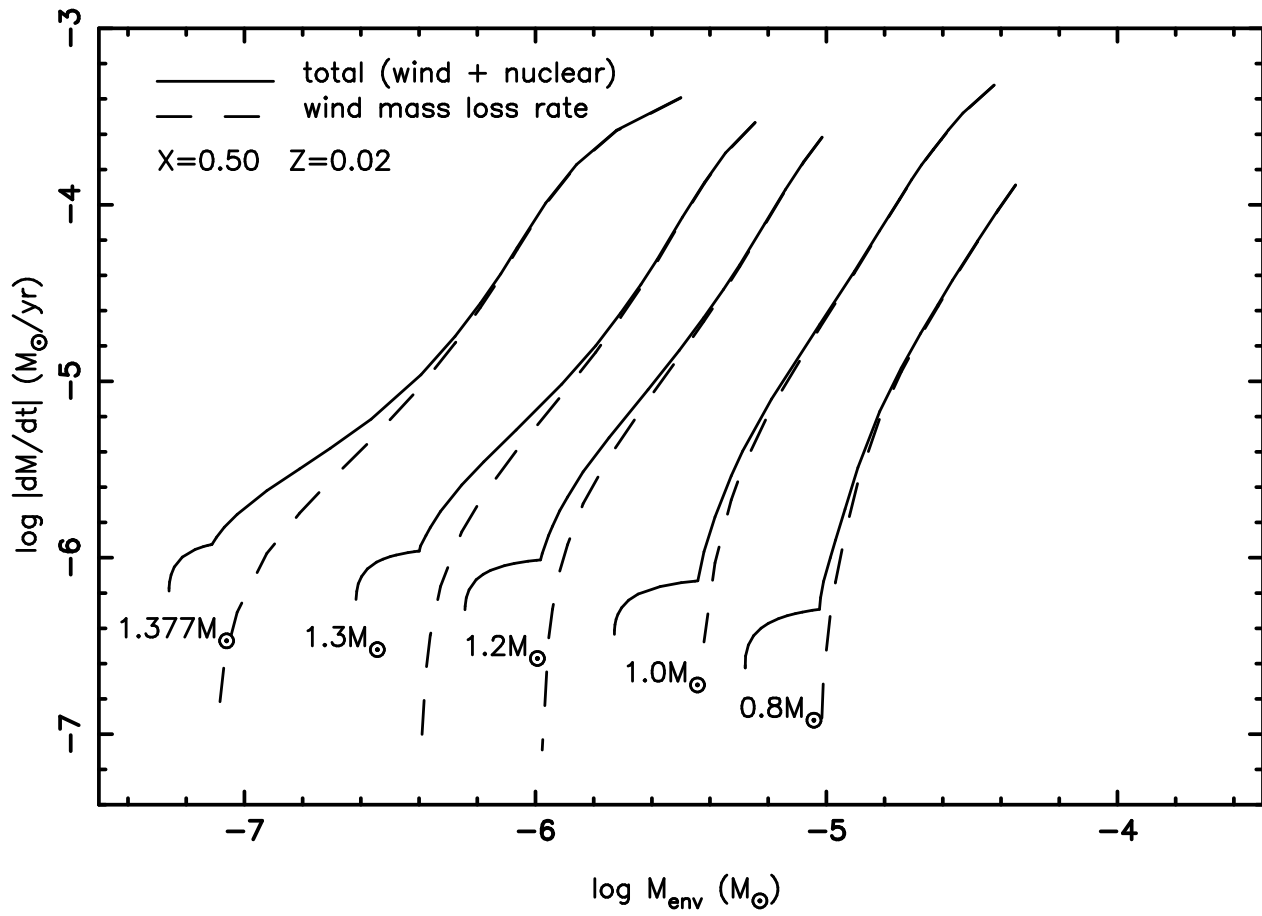


FIG. 5.— Wind mass loss rate (dashed line) and envelope mass decreasing rate (solid line), i.e., nuclear burning rate plus wind mass loss rate, are plotted against the envelope mass for white dwarfs with mass of 0.8, 1.0, 1.2, 1.3 and $1.377M_{\odot}$. The white dwarf mass is attached to each line. There exist only static solutions below the break on each solid line while optically thick winds blow above the break.

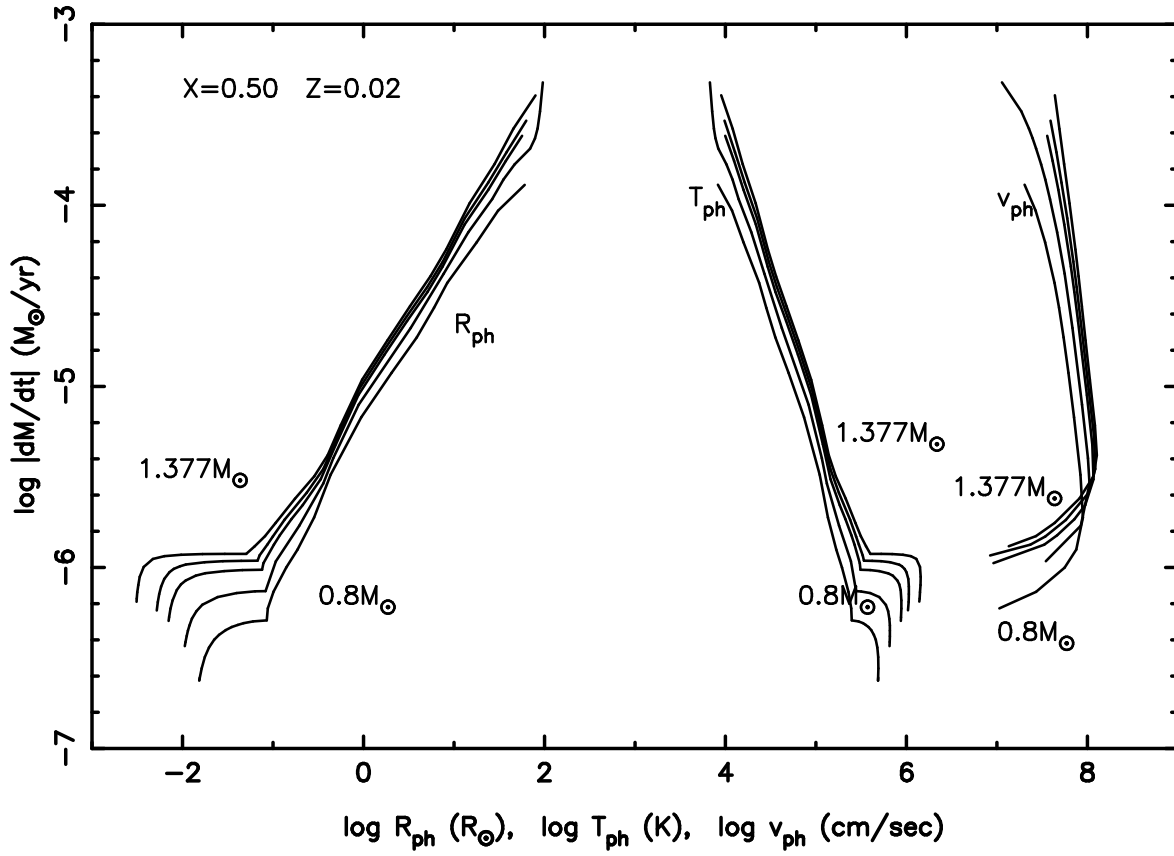


FIG. 6.— Photospheric radius (R_{ph}), temperature (T_{ph}), and velocity (v_{ph}) are plotted against the envelope mass decreasing rate (i.e., nuclear burning rate plus wind mass loss rate) for five cases of the white dwarf mass, $M_{\text{WD}} = 0.8, 1.0, 1.2, 1.3$ and $1.377M_{\odot}$. There exist only static solutions below the break on each solid line of the photospheric temperature and radius while optically thick winds blow above the break. Photospheric velocity is plotted only for wind solutions.

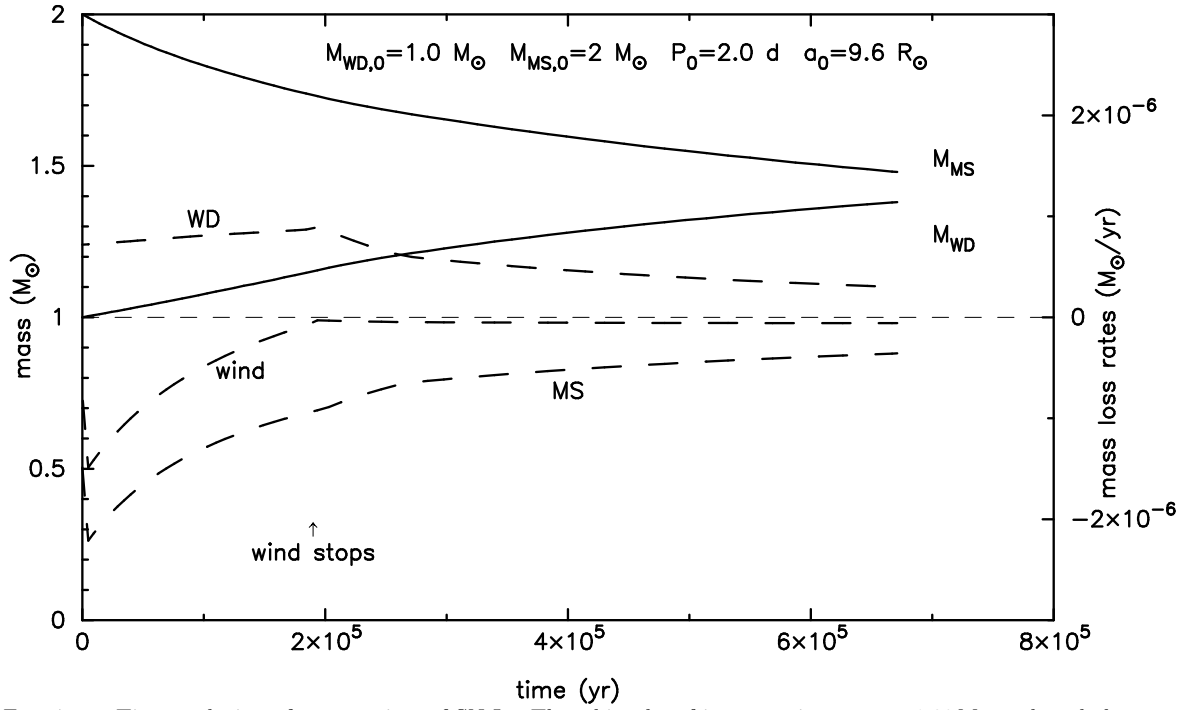


FIG. 7.— Time evolution of a progenitor of SN Ia. The white dwarf increases its mass to $1.38M_\odot$ and explodes as an SN Ia. Solid lines denote the masses of the white dwarf (M_{WD}) and the main-sequence companion (M_{MS}). The dashed lines denote, from top to bottom, the net mass accretion rate onto the white dwarf (denoted by “WD”), the wind mass loss rate (denoted by “wind”), and the mass decreasing rate of the companion (denoted by “MS”), respectively. The dashed line shows the average mass loss rate of $\sim 6 \times 10^{-8} M_\odot \text{ yr}^{-1}$ due to helium shell flashes after “wind stops.”

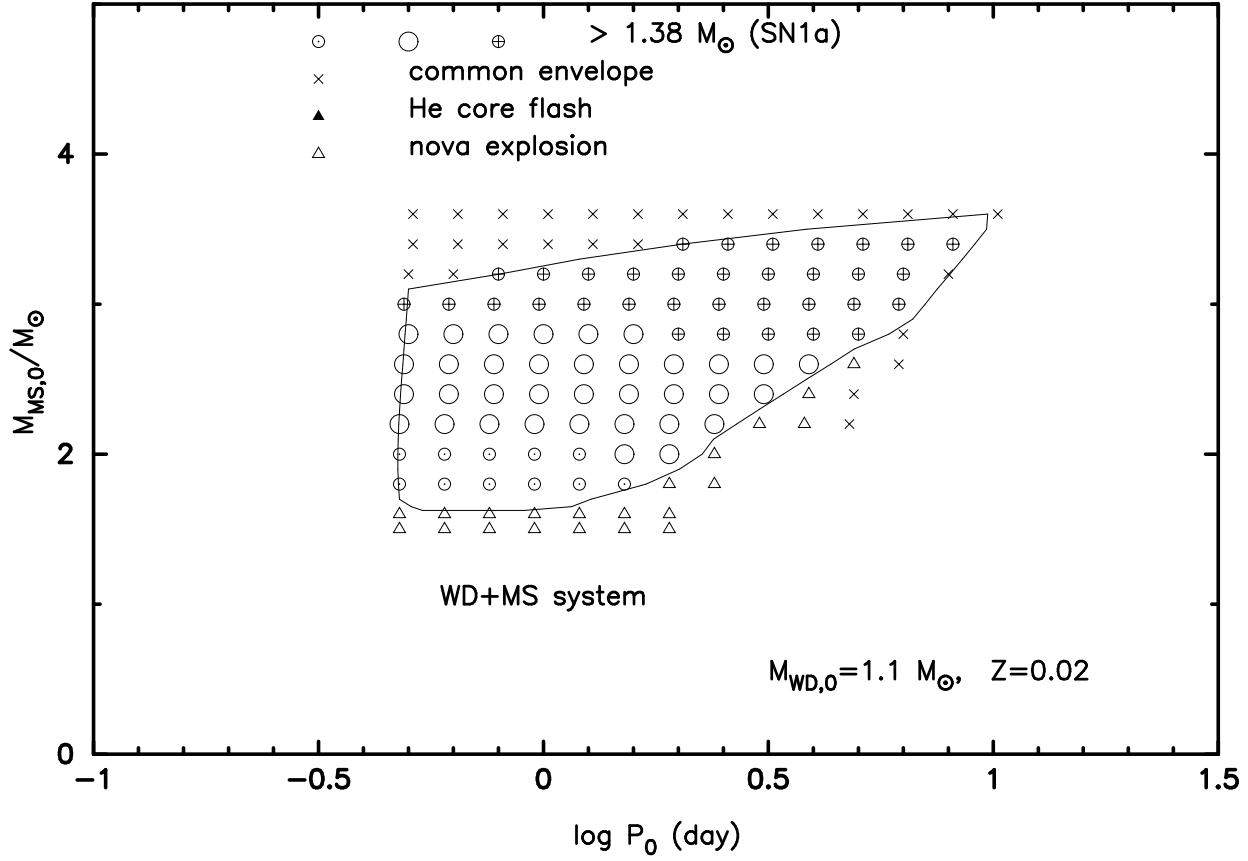


FIG. 8.— Final outcome of close binary evolution in the $\log P_0 - M_{\text{MS},0}$ plane for $M_{\text{WD},0} = 1.1 M_\odot$. Final outcome is either 1) forming a common envelope (denoted by \times) because the mass transfer rate at the beginning is large enough to form a common envelope, i.e., $R_{\text{ph}} \gtrsim 10 R_\odot$ for $\dot{M}_2 \gtrsim 1 \times 10^{-4} \text{ yr}^{-1}$ as seen in Fig. 6, 2) triggering an SN Ia explosion (denoted by \oplus , \bigcirc , or \odot) when $M_{1,\text{WD}} = 1.38 M_\odot$ or 3) triggering repeated nova cycles (denoted \triangle), i.e., $\dot{M}_2 < \dot{M}_{\text{low}}$ when $M_{1,\text{WD}} < 1.38 M_\odot$. Among the SN Ia cases, the wind status at the explosion depends on \dot{M}_2 as follows. 2a) Wind continues at the SN Ia explosion for $\dot{M}_{\text{cr}} < \dot{M}_2 \lesssim 1 \times 10^{-4} M_\odot \text{ yr}^{-1}$ (\oplus). 2b) Wind stops before the SN Ia explosion but the mass transfer rate is still high enough to keep steady hydrogen shell burning for $\dot{M}_{\text{st}} < \dot{M}_2 < \dot{M}_{\text{cr}}$ (\bigcirc). 2c) Wind stops before the SN Ia explosion and the mass transfer rate decreases to between $\dot{M}_{\text{low}} < \dot{M}_2 < \dot{M}_{\text{st}}$ at the SN Ia explosion (\odot). The region leads to SN Ia explosions is bounded by the solid line.

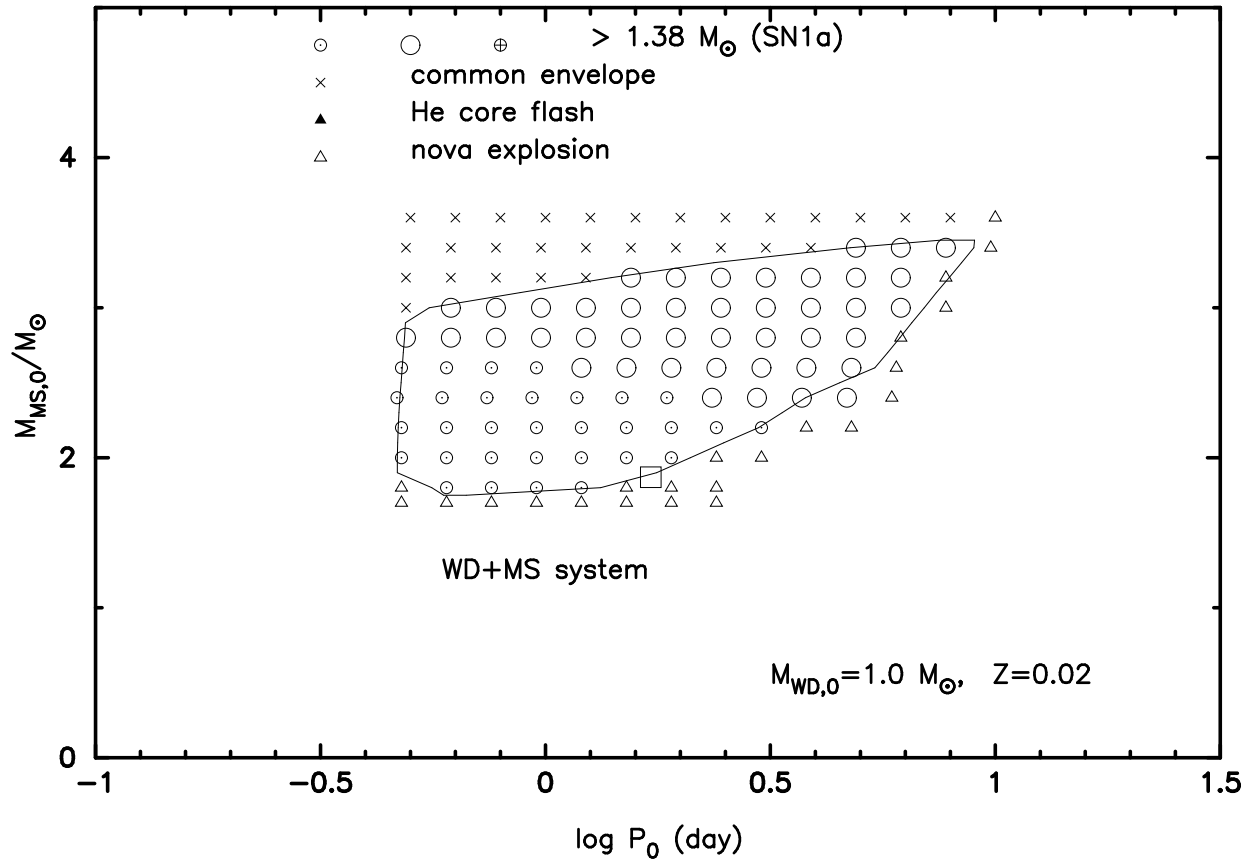


FIG. 9.— Same as in Fig. 8 but for $M_{\text{WD},0} = 1.0 M_{\odot}$. A box mark (\square) denotes an initial binary parameter of U Sco.

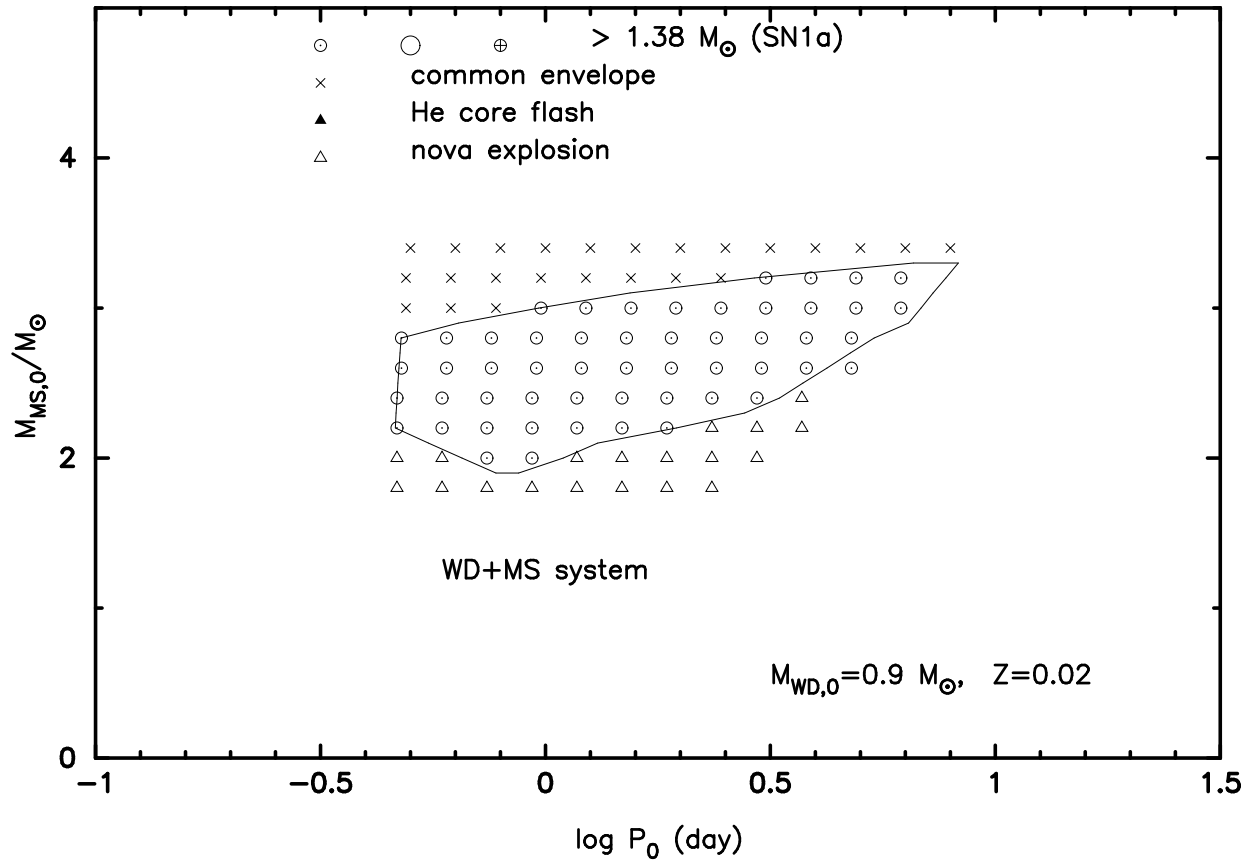


FIG. 10.— Same as in Fig. 8 but for $M_{\text{WD},0} = 0.9 M_{\odot}$.

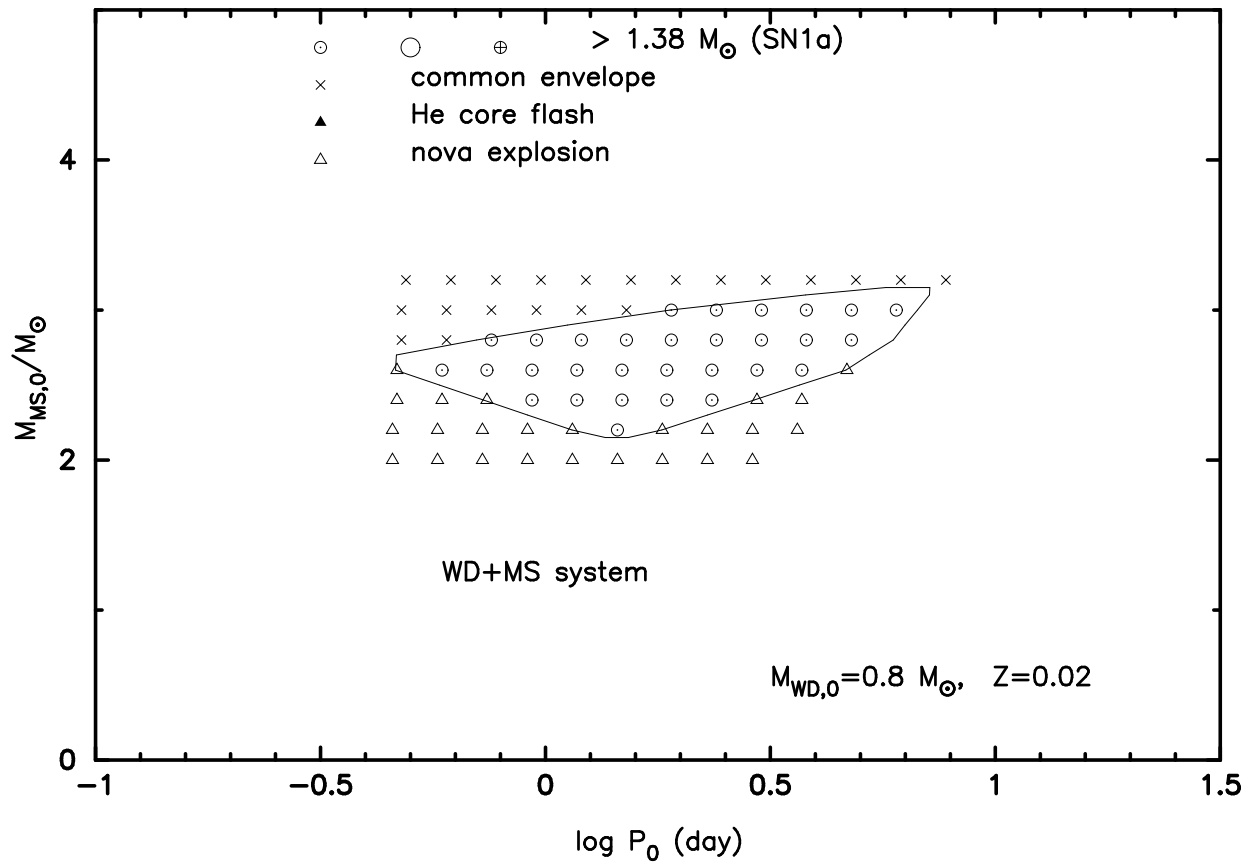


FIG. 11.— Same as in Fig. 8 but for $M_{\text{WD},0} = 0.8 M_{\odot}$.

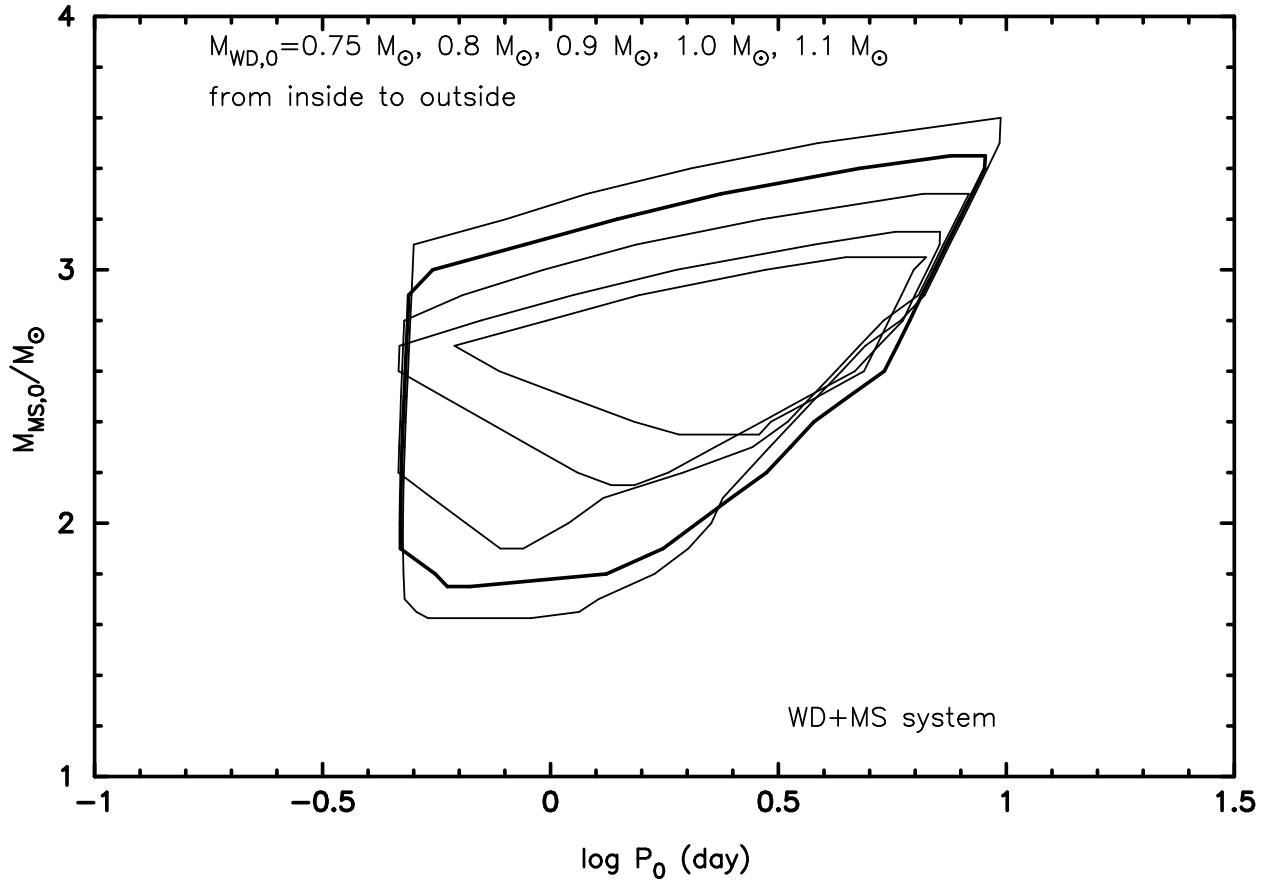


FIG. 12.— Regions that lead to SN Ia explosions are plotted in the $\log P_0 - M_{\text{MS},0}$ plane for five cases of the initial white dwarf mass, i.e., $M_{\text{WD},0} = 0.75, 0.8, 0.9$, and $1.1 M_\odot$ (thin solid) together with $M_{\text{WD},0} = 1.0$ (thick solid). The region for $M_{\text{WD},0} = 0.7 M_\odot$ vanishes, however.